ORIGINAL ARTICLE

Intrapulmonary unicentric Castleman's disease: A clinical analysis of 8 patients

LINLING JIN[1*], YITING HE[2*], CHENYANG LIU[3*], SONGTAO LIU[1], SHUYING MA[4], NAN LI[1], HUI KONG[1], WEIPING XIE[1], MENGYU HE[1]

[1]Department of Pulmonary and Critical Care Medicine, The First Affiliated Hospital of Nanjing Medical University, Nanjing, Jiangsu, China; [2]Department of Respiratory and Critical Care Medicine, Nanjing First Hospital, Nanjing Medical University, Nanjing, Jiangsu, China; [3]Department of Respiratory and Critical Care Medicine, Affiliated People's Hospital of Jiangsu University, Zhenjiang, Jiangsu, China; [4]Department of Pathology, The First Affiliated Hospital of Nanjing Medical University, Nanjing, Jiangsu, China.

*These authors contributed equally to the work.

ABSTRACT

Background and aims: Castleman's disease (CD) is a rare, chronic, lymphoproliferative disorder, increasingly recognized as a clonal neoplasm of lymph node stromal cells that can affect multiple organs and tissues. Intrapulmonary unicentric Castleman's disease (UCD) represents an exceptionally uncommon subtype, primarily involving the lung parenchyma and hilum, with only a few pathologically confirmed cases reported to date. This study aimed to characterize the clinical, radiological, and pathological features of intrapulmonary UCD and to summarize diagnostic and therapeutic experiences.

Methods: We retrospectively analyzed eight patients diagnosed with intrapulmonary UCD. Clinical manifestations, laboratory data, radiologic and bronchoscopic findings, histopathological characteristics, treatment approaches, and follow-up outcomes were systematically reviewed.

Results: No patient exhibited specific clinical symptoms or distinctive laboratory abnormalities. Chest computed tomography (CT) served as the optimal imaging modality, consistently revealing solitary, well-circumscribed, soft-tissue masses with smooth lobulated contours. Definitive diagnosis relied on histopathological examination. All patients underwent complete surgical resection, followed by regular postoperative surveillance with chest CT. During follow-up, no local recurrence or disease progression was detected.

Conclusions: Intrapulmonary UCD is an exceedingly rare form of Castleman's disease that can be easily misdiagnosed as primary lung tumors, lymphoma, granulomatous disease, or tuberculosis due to its nonspecific clinical

Received: 20 October 2025 | Accepted: 1st January 2026

Correspondence: Mengyu He / Department of Pulmonary and Critical Care Medicine, The First Affiliated Hospital of Nanjing Medical University, 300 Guangzhou Road, Nanjing, Jiangsu 210029, China /
E-mail: myhe@njmu.edu.cn

and radiological features. Complete surgical excision remains the mainstay of treatment and is associated with an excellent prognosis following complete resection.

Key words: unicentric Castleman's disease, intrapulmonary lesion, clinical features, surgical resection

Introduction

Castleman's disease (CD) is a rare and heterogeneous group of lymphoproliferative disorders. Recent molecular evidence suggests Unicentric Castleman's Disease (UCD), particularly the hyaline vascular variant, may represent a clonal neoplastic proliferation of follicular dendritic cells, rather than a purely reactive process (1). The first confirmed case of CD was reported by Benjamin Castleman in 1954 (2). On the basis of the regional involvement of lymph nodes, CD can be clinically classified into two types: unicentric Castleman's disease (UCD) and multicentric Castleman's disease (MCD) (3). UCD accounts for 68%-96% of all cases of CD (4). The most frequent sites of UCD include the cervical region, mediastinum, pulmonary hilum, and abdominal cavity (5). However, intrapulmonary UCD is extremely uncommon, with only a few confirmed cases reported to date (5). The diagnosis of intrapulmonary UCD is challenging due to the nonspecific clinical manifestations of the disease, which often lead to potential misdiagnosis as lymphoma, neoplasm, or infection (6). The aim of this study is to provide a detailed analysis of the clinical data of 8 patients who were diagnosed with intrapulmonary UCD, with a focus on their clinical features, treatment approaches, and prognoses, to increase our knowledge of this condition.

Methods

Study design

This study included a total of 8 hospitalized patients with intrapulmonary UCD confirmed via surgical pathology between January 2017 and December 2023. Data encompassing clinical manifestations, symptoms, laboratory test results, and radiological images were collected from electronic medical records. We also obtained clinical information from the patients or their family members. Additional data regarding treatment response, outcomes, and pertinent follow-up details were likewise gathered. Ethical approval for this study was obtained from the First Affiliated Hospital with Nanjing Medical University (2024-SR-877), which waived the requirement for informed consent due to the retrospective study design.

H&E staining and immunohistochemical staining

The excised samples were fixed in a 3.7% neutral formaldehyde solution, dehydrated, embedded in paraffin, and sectioned at a thickness of 4 μm. The sections were subsequently subjected to hematoxylin□eosin (H&E) staining and immunohistochemical staining with primary antibodies against CD3, CD20, CD79a, Mum-1, CD38, CD138, kappa and lambda light chains as well as CD21, CD23 and Ki67.

Statistical analysis

The data are expressed as means ± standard deviations ($\bar{x}$ ±s) for continuous variables and frequency with percentage (%) for categorical variables.

Results

Clinical features

Among 8 patients who were diagnosed with intrapulmonary UCD, 3 (37.5%) were male and 5 (62.5%) were female, resulting in a male-to-female ratio of 0.6:1. The mean age was 39.6±16.8 years (Table 1).

Table 1. The clinical characteristics of the 8 patients who developed intrapulmonary Unicentric Castleman's Disease

Clinical parameters	n=8
Age (year) ($\bar{x}$±s)	39.6 ± 16.8
Sex (male) [n (%)]	3 (37.5%)
Clinical symptoms [n (%)]	
Chest tightness	3 (37.5%)
Cough	1 (12.5%)
Chest pain	1 (12.5%)
None	4 (50.0%)
Treatment [n (%)]	
Surgery	8 (100.0%)
Outcome [n (%)]	
Surviving	8 (100.0%)
Recurrence	0 (0)

Among the 8 patients, 4 were referred to the hospital because they were noted as having an abnormal shadow on chest computed tomography (CT) images at a health checkup without any symptoms. Three (37.5%) patients experienced chest tightness, 1 (12.5%) had a cough, and 1 (12.5%) presented with chest pain accompanied by a sensation of thoracic heaviness. All of the patients underwent physical examination at admission, which revealed no palpable superficial lymph nodes (Table 1).

Laboratory features

Prior to treatment, all patients had normal peripheral white blood cell counts, lymphocyte counts, neutrophil counts, platelet counts, hemoglobin levels, lactate dehydrogenase levels, serum albumin levels and serum globulin levels. Among these 8 patients, 1 presented with anemia (113 g/L), 1 had elevated D-dimer levels (1.57 μg/mL), and 2 had significantly increased IL-6 levels prior to treatment. Surgical treatment resulted in a reduction in the IL-6 level, which subsequently returned to baseline.

Imaging features

All patients underwent chest CT examination, with CT values ranging from 30 to 48 HU (Figure 1a-b; Table 2). Among these, 2 lesions were located in the right hilum, 4 in the left hilum, and 2 in the right inferior lobe. The lesions appeared as smooth, rounded or oval soft tissue shadows with well-defined edges and no irregularities. The maximum diameter was 4.0±1.4 cm, and the lesions exhibited significant and diverse enhancement after contrast-enhanced scanning. In addition to the aforementioned manifestations, localized enlargement of mediastinal lymph nodes was observed in 5 patients, whereas punctate, branching or coarse calcifications within the lesions were found in 2 patients. Other imaging findings included one case where the lesion encased the right upper lobe pulmonary artery and bronchus and another case where the bronchus was visible within the lesion itself. Two patients had small ipsilateral ground-glass nodules adjacent to the main mass, likely representing secondary changes. Two other patients had small amounts of bilateral pleural effusion. One patient presented with nourishing blood vessels. One patient underwent preoperative high-resolution 3T lung magnetic resonance imaging (MRI) with both plain scans and contrast enhancement, revealing a patchy T2 hyperintense ring-shaped lesion at the right pulmonary hilum. The lesion exhibited a ring-shaped hyperintense signal on T1-weighted images and diffusion-weighted imaging (DWI), accompanied by a slightly decreased apparent diffusion coefficient (ADC) value (***Figure 1c-d***). Additionally, the enhanced curve exhibited a rapid increase followed by a plateau. One patient underwent PET/CT examination with an intravenous injection of ^{18}F-fluorodeoxyglucose (FDG) for whole-body and brain imaging. The PET/CT scan revealed heterogeneous increased radioactive uptake in the lung lesions, with a maximum standardized uptake value (SUVmax) of 5.6 (Figure 1e-f).

Bronchoscopic characteristics

Four patients underwent electronic bronchoscopy, which revealed clear and smooth lumens of the main bronchus and various segmental bronchi without any evidence of bleeding or neoplasms. Subsequent endobronchial ultrasound examination revealed enlarged lymph nodes with well-defined boundaries, heterogeneous internal echoes, and minimal vascularity. Fine needle aspiration was conducted, and cytological analysis of the fluid sample revealed a small number

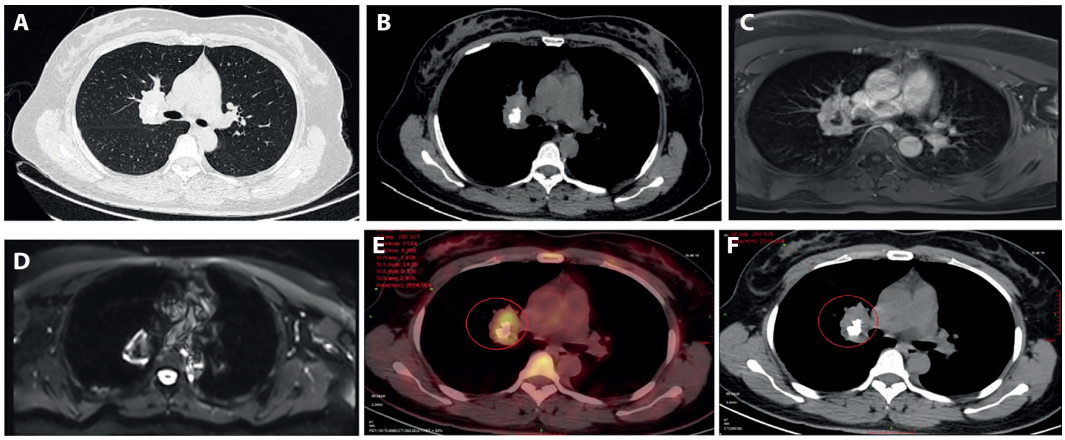

Figure 1. Imaging characteristics of intrapulmonary unicentric Castleman's disease. (a-b) Chest CT revealed a mass with soft tissue density and calcification in the right pulmonary hilum. MRI revealed the presence of a circular high signal in the hilum of the right lung, which was observed on both T1-weighted (c) and diffusion-weighted (d) images. (e-f) PET/CT revealed an irregular mass with coarse calcification within the right upper pulmonary hilus, encompassing the pulmonary artery and bronchus in the right upper lobe of the lung.

Table 2. The imaging characteristics of the 8 patients who developed intrapulmonary Unicentric Castleman's Disease

No.	Location	Diameter (cm)	Mediastinal lymphadenopathy	GGO	Calcification	Boundary	Pleural effusion
1	Right pulmonary hilar	4.5	Yes	Yes	No	clear	No
2	Right pulmonary hilar	3.7	No	No	Yes	clear	No
3	Left pulmonary hilar	4.0	Yes	No	No	clear	No
4	Left pulmonary hilar	3.8	Yes	No	No	clear	Yes
5	Left pulmonary hilar	4.5	No	Yes	Yes	clear	Yes
6	Left pulmonary hilar	3.6	No	No	No	clear	No
7	Right lower lobe	6.7	Yes	No	No	clear	No
8	Right lower lobe	1.3	Yes	No	No	clear	No

Abbreviations: GGO, Ground-glass nodules

of atypical cells. Histopathological examination of the biopsy specimen revealed fragmented and compressed lymphoid tissue with minor hemorrhage.

Pathological features

Histopathological examination of all eight resected specimens confirmed the diagnosis of the hyaline vascular variant (HVV) of Castleman disease. The cardinal features included an abnormal follicular architecture, characterized by numerous lymphoid follicles with markedly expanded mantle zones. These mantle zones were composed of concentric layers of small lymphocytes arranged in an "onion-skin" pattern, surrounding regressively transformed germinal centers. Accompanying this was a prominent interfollicular vascular proliferation of small hyalinized vessels, which frequently penetrated into the atrophic germinal

centers to form the pathognomonic "lollipop" lesions (Figure 2b). Immunohistochemically, stains for CD21 highlighted a prominent and expanded meshwork of follicular dendritic cells within these atrophic centers and extending into the mantle zones (Figure 2e). Additionally, scattered clusters of plasmacytoid dendritic cells were identified in the interfollicular regions.

Clinical treatment and outcomes

All patients underwent thoracoscopic surgery for complete resection of the lesions. Intraoperatively, all lesions were identified as solid masses with intact capsules. Follow-up examinations were performed until December 31, 2023, with an average follow-up duration of 35.5±32.0 months, and all patients exhibited complete remission (Table 1).

Discussion

CD, known as a chronic lymphoproliferative disorder, is also referred to as giant lymph node hyperplasia. UCD represents the most prevalent form of CD (7). However, more than 70% of UCD cases exhibit thoracic involvement, particularly mediastinal involvement. In rare cases, UCD is observed in the lungs and is termed intrapulmonary UCD. Owing to nonspecific laboratory and imaging findings, intrapulmonary UCD is often misdiagnosed as lung tumors, lymphoma, granulomas or tuberculous infections (8). Previous studies revealed that CD can manifest at any age, with a median age at onset of approximately 40 years for MCD patients, indicating that individuals are older at the time of MCD onset than individuals are at the time of UCD onset (9). The overall incidence rate of UCD surpasses that of MCD, and there are no significant sex-specific differences (10). The mean age in this study was 39.6±16.8 years, with a median age at onset of 36 years and a male-to-female ratio of 0.6:1, which is consistent with previous studies (9,10). In addition, specific clinical manifestations are not commonly observed in CD patients (11). Most cases of UCD with chest involvement typically remain asymptomatic and are commonly identified

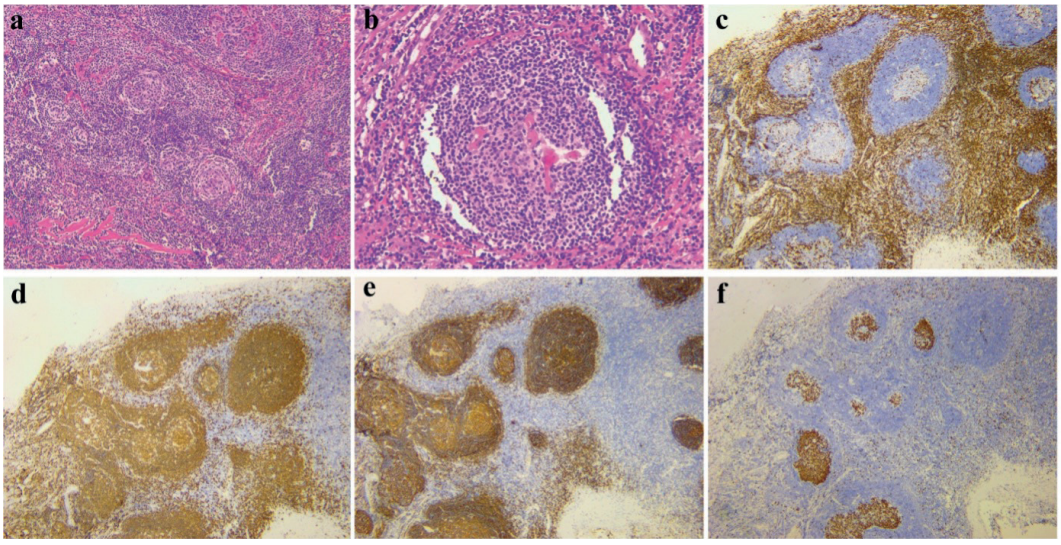

Figure 2. H&E staining and immunohistochemical staining of intrapulmonary unicentric Castleman's disease. (a, b) H&E staining demonstrating the histologic hallmarks of the hyaline vascular variant, including lymphoid follicles with regressively transformed germinal centers and markedly expanded mantle zones exhibiting concentric "onion skin-like" layering of small lymphocytes (a, ×100). A characteristic hyalinized vessel penetrating a germinal center to form a "lollipop" lesion is indicated by an arrow (b, ×200). (c–f) Immunohistochemistry reveals CD3-positive T cells in the interfollicular and outer mantle zones (c, ×40), CD20-positive B cells within follicular centers (d, ×40), a prominent and expanded meshwork of CD21-positive follicular dendritic cells within the atrophic germinal center (e, ×40), and high Ki67 expression indicating active proliferation (f, ×40).

Table 3. The Pathological features of the 8 patients who developed intrapulmonary Unicentric Castleman's Disease

NO. / Marker	1	2	3	4	5	6	7	8
Pathological type	HVV	HVV	HVV	HVV	HVV	HVV	HVV	HVV
CD3	+	+	+	+	+	+	+	-
CD20	+	+	+	+	+	+	+	+
CD79a	+	+	+	/	+	+	-	/
MUM1	/	/	+	/	/	+	+	/
CD38	+	+	+	/	+	+	+	+
CD138	-	-	+	/	-	+	-	/
Kappa	+	+	-	/	+	+	+	+
Lambda	+	+	-	/	+	-	+	+
CD21	+	+	+	+	+	+	+	+
CD23	+	+	+	+	+	+	/	/
Ki67	+	+	+	+	+	+	+	+

Abbreviations: HVV, homogeneous hyaline vascular variant

through routine examinations or subsequent medical consultations regarding the presence of pulmonary lesions. Some patients seek medical attention when they experience compression symptoms caused by the lesion, such as coughing, difficulty breathing, hemoptysis, dysphagia, or recurrent pneumonia. When the lesion is located in the chest wall area, it may present as localized pain within the tumor region. If the lesion extends to regions such as the axillary or supraclavicular areas or the superior thoracic inlet into the mediastinum, it may be palpable during physical examination (12). In this study, approximately 50% of the patients (4/8) presented with an abnormal CT shadow during a health checkup, despite being asymptomatic. The remaining four patients experienced mild chest tightness, chest pain or coughing. By correlating their chest CT scans, it was hypothesized that these symptoms may be attributed to significant mass compression on the trachea, blood vessels, or lung tissue. Regarding laboratory findings, while none of our patients exhibited systemic inflammatory markers typically associated with MCD, two did present with elevated serum IL-6 levels preoperatively. Importantly, these levels normalized following surgical resection. While elevated serum IL-6 is characteristic of MCD, mild elevation can occasionally be observed in UCD, potentially reflecting localized cytokine production by the lesion itself rather than a systemic disorder. In our series, the postoperative normalization of IL-6 supports its origin from the resected unicentric mass, thereby distinguishing these cases from true systemic MCD. Imaging plays a pivotal role in the detection of UCD. Chest CT is the preferred imaging modality for evaluating lesions in UCD patients (13). On CT, UCD typically presents as solitary soft tissue masses measuring five to seven cm in maximum diameter, on average. Furthermore, CT consistently reveals well-defined borders and smooth lobulation of these solitary soft tissue masses. Occasionally, calcification or infiltration into adjacent fat or structures may be observed. Pleural effusion can sometimes accompany UCD. After the administration of contrast agent for enhanced CT, these lesions often exhibit heterogeneous enhancement patterns and a dramatic increase in enhancement during the arterial phase, which persists but decreases during the portal venous phase (4). The features of UCD on MRI images are relatively similar, but often nonspecific, to those of UCD on CT images. T1-weighted postcontrast images consistently show intense enhancement and heterogeneity due to necrotic, edematous, or fibrotic areas (13). UCD causes a moderate increase in uptake on PET/CT, with a wide range of reported standardized uptake values (SUVs) (14). Although these finding

lacks specificity, it could assist in narrowing the differential diagnosis by excluding malignancies and assessing systemic involvement. In this study, we observed a concordance between the imaging features of intrapulmonary UCD and those reported in studies on UCD. For unexplained lung masses, CT-guided percutaneous lung puncture biopsy or EBUS can be performed for pathological diagnosis. EBUS, as an innovative technology, serves as a valuable enhancement and complement to traditional methods because of its safety and feasibility. EBUS is particularly suitable for lesions near the hilum of the lung or those associated with enlarged mediastinal lymph nodes. However, both aforementioned techniques yield small specimens of pathological tissue, sometimes leading to inconclusive diagnoses. For hilar or mediastinal lesions, bronchoscopic techniques play a crucial diagnostic role. While EBUS-guided fine-needle aspiration is widely used, its yield for diagnosing CD can be limited due to the architectural tissue requirement. Recent advancements, such as EBUS-guided cryobiopsy or core needle biopsy, allow for the retrieval of larger tissue specimens, preserving the lymph node architecture necessary for the histopathological diagnosis of CD (15). This approach can serve as a less invasive alternative to surgical biopsy in select cases, potentially confirming the diagnosis prior to definitive surgical resection. Surgical excision is the primary treatment for UCD. On one hand, it allows for the acquisition of sufficient specimens to facilitate definitive diagnosis; on the other hand, it enables lesion excision and the alleviation of compression-related symptoms (16). In this study, 8 patients underwent surgical excision. Among them, two patients underwent EBUS puncture prior to surgery, and the pathological findings indicated that manipulation of disrupted lymphoid tissue could aid in excluding granulomatous diseases and malignant tumors. The diagnosis of Castleman's disease is primarily established through histopathological evaluation. Pathologically, CD can be classified into two subtypes: the hyaline vascular variant (HVV) and the plasma cell variant (PCV). HVV is more likely to present as unicentric, whereas PCV is commonly observed as multicentric (4). In this study, all 8 patients were diagnosed with HVV pathologically. The most distinctive characteristic of UCD is the expansion of mantle zones characterized by the presence of multiple concentric rings composed of lymphocytes surrounding atretic follicles—commonly referred to as targetoid or onion-skin mantle cells (17). All 8 patients in this study underwent immunohistochemical examination, and most patients exhibited positive staining for CD3, CD20, CD79a, Mum-1, CD38, CD138, kappa, lambda, CD21, CD23 and Ki67 (Table 3). The preferred treatment for UCD is surgical resection because of its favorable therapeutic efficacy and lower recurrence rates. Preoperative evaluation of the vascular supply and drainage surrounding the lesion is highly important. In cases in which complete resection cannot be achieved or when surgical contraindications are present, low-dose radiation therapy is frequently chosen (18). The prognosis following surgical resection of UCD is favorable. In this study, 8 patients underwent regular postoperative follow-up chest CT examinations, which revealed no evidence of lesion recurrence. In conclusion, intrapulmonary UCD is a rare variant of UCD that primarily affects the hilum and lung. Intrapulmonary UCD often presents with nonspecific clinical manifestations and is predominantly characterized by HVV. Surgical excision remains the preferred therapeutic approach for this type of lesion. Given its nonspecific clinical presentations and imaging features, accurate differential diagnosis is crucial. In the future, a multicenter study on intrapulmonary UCD would be beneficial for elucidating specific disease aspects and increasing clinicians' knowledge of the disease, which will decrease the risks of missed diagnoses and misdiagnoses.

Data availability: The datasets used and analyzed in the current study are available from the corresponding author upon reasonable request.

Conflict of interest: Each author declares that he or she has no commercial associations that might pose a conflict of interest in connection with the submitted article.

Acknowledgements: This work was funded by grants from Young Scholars Fostering Fund of the First Affiliated Hospital of Nanjing Medical University (Grant No. PY2022012) and the Jiangsu Province Capability Improvement Project through

Science, Technology and Education; Jiangsu Provincial Medical Innovation Center (Grant No. CXZX202206).

Declaration on the use of AI: The authors confirm that no AI-generated text, data, or insights were incorporated into this work, and that all content reflects the original contributions and responsibilities of the authors.

References

1. Wang S, Wang R, Shang P, et al. Whole-exome sequencing reveals the genomic profile and IL6ST variants as a prognostic biomarker of paraneoplastic pemphigus-associated unicentric Castleman disease. J Invest Dermatol. 2024;144(3):585–92. doi:10.1016/j.jid.2023.07.031
2. Inada K, Hamazaki M. Localized mediastinal lymph-node hyperplasia resembling thymoma; a case report. Ann Surg. 1958;147(3):409–13. doi:10.1097/00000658-195803000-00018
3. Dispenzieri A, Fajgenbaum DC. Overview of Castleman disease. Blood. 2020;135(16):1353–64. doi:10.1182/blood.2019000931
4. Kligerman SJ, Auerbach A, Franks TJ, et al. Castleman disease of the thorax: clinical, radiologic, and pathologic correlation: from the radiologic pathology archives. Radiographics. 2016;36(5):1309–32. doi:10.1148/rg.2016160076
5. Hoffmann C, Hentrich M, Tiemann M, et al. Recent advances in Castleman disease. Oncol Res Treat. 2022;45(11):693–704. doi:10.1159/000526640
6. Liu Y, Chen G, Qiu X, et al. Intrapulmonary unicentric Castleman disease mimicking peripheral pulmonary malignancy. Thorac Cancer. 2014;5(6):576–80. doi:10.1111/1759-7714.12129
7. AlSheikh S, Altoijry A, Al-Mubarak H, et al. A rare presentation of unicentric Castleman's disease in the thigh: a case report and review of literature. World J Clin Cases. 2024;12(19):4003–9. doi:10.12998/wjcc.v12.i19.4003
8. Fuentes GC, López SS, González AS, et al. Unicentric Castleman's disease mimicking an hilar lung cancer. Cir Esp. 2023;101(4):298–300. doi:10.1016/j.cireng.2022.06.004
9. Pertusa Mataix R, Loaiza Cabello D, García Morillo JS. Castleman's disease, pathophysiology, advances in diagnosis and treatment. Med Clin (Barc). 2024;162(6):283–90. doi:10.1016/j.medcli.2023.10.013
10. Dispenzieri A, Armitage JO, Loe MJ, et al. The clinical spectrum of Castleman's disease. Am J Hematol. 2012;87(11):997–1002. doi:10.1002/ajh.23291
11. Haap M, Wiefels J, Horger M, et al. Clinical, laboratory and imaging findings in Castleman's disease - the subtype decides. Blood Rev. 2018;32(3):225–34. doi:10.1016/j.blre.2017.11.005
12. Hu S, Li Z, Wang H, et al. Clinical features and treatment outcomes of Castleman disease in children: a retrospective cohort in China. Eur J Pediatr. 2023;182(12):5519–30. doi:10.1007/s00431-023-05235-2
13. Pitot MA, Tahboub Amawi AD, Alexander LF, et al. Imaging of Castleman disease. Radiographics. 2023;43(8):e220210. doi:10.1148/rg.220210
14. He L, Chen Y, Tan X, et al. (18)F-FDG PET/CT and contrast-enhanced CT in the diagnosis of Castleman disease. Jpn J Radiol. 2023;41(1):98–107. doi:10.1007/s11604-022-01318-6
15. Poletti V, Petrarulo S, Piciucchi S, et al. EBUS-guided cryobiopsy in the diagnosis of thoracic disorders. Pulmonology. 2024;30(5):459–65. doi:10.1016/j.pulmoe.2023.11.008
16. Pertusa Mataix R, Loaiza Cabello D, García Morillo JS. Castleman's disease, pathophysiology, advances in diagnosis and treatment. Med Clin. 2024;162(6):283–90. doi:10.1016/j.medcli.2023.10.013
17. Molacek J, Treska V, Skalicky T, et al. Unicentric form of Castlemans disease, pitfalls of diagnosis and surgical treatment. Front Oncol. 2023;13:1057683. doi:10.3389/fonc.2023.1057683
18. Mitsos S, Stamatopoulos A, Patrini D, et al. The role of surgical resection in unicentric Castleman's disease: a systematic review. Adv Respir Med. 2018;86(1):36–43. doi:10.5603/ARM.2018.0008